Check for updates

AGU100 ADVANCING EARTH AND SPACE SCIENCE

Water Resources Research

RESEARCH ARTICLE
10.1029/2018WR022989

Key Points:
- We present a new methodology to quantify groundwater storage changes driven by snowmelt in high alpine catchment with limited access
- Airborne quantification of premelt snow volumes is a key to quantify seasonal groundwater storage changes using a water balance approach
- Substantial groundwater storage highlights the potential of alpine aquifers to seasonally redistribute water and stabilize streamflow

Supporting Information:
- Supporting Information S1

Correspondence to:
D. Hunkeler,
daniel.hunkeler@unine.ch

Citation:
Cochand, M., Christe, P., Ornstein, P., & Hunkeler, D. (2019). Groundwater storage in high alpine catchments and its contribution to streamflow. *Water Resources Research*, *55*, 2613–2630. https://doi.org/10.1029/2018WR022989

Received 21 MAR 2018
Accepted 18 FEB 2019
Accepted article online 25 FEB 2019
Published online 2 APR 2019

©2019. The Authors.
This is an open access article under the terms of the Creative Commons Attribution-NonCommercial-NoDerivs License, which permits use and distribution in any medium, provided the original work is properly cited, the use is non-commercial and no modifications or adaptations are made.

Groundwater Storage in High Alpine Catchments and Its Contribution to Streamflow

M. Cochand[1], P. Christe[2], P. Ornstein[3], and D. Hunkeler[1]

[1]Centre for Hydrogeology and Geothermics (CHYN), University of Neuchâtel, Neuchâtel, Switzerland, [2]Environmental Agency, Canton du Valais, Sion, Switzerland, [3]CREALP, Sion, Switzerland

Abstract There is limited knowledge about groundwater storage in alpine catchments, although it might strongly influence how these catchments react to earlier snowmelt due to climate change. The objective of the study was to develop and test a method to quantify seasonal groundwater storage in alpine catchments and evaluate how groundwater storage is related to hydrogeological properties. As representative water table observations are challenging to acquire in such environments, we used a water balance approach targeting the main snowmelt period when most groundwater recharge is expected to occur. Based on a detailed quantification of the snow water equivalent at the onset of snowmelt combined with discharge measurements, it is possible to quantify groundwater storage with a low uncertainty even if other terms of the water balance are less well constrained. The application of the method to an 11-km^2 research catchment revealed a large seasonal increase of groundwater storage by 300 mm or 45% of the premelt snow water equivalent. An independent quantification of groundwater storage depletion during the 7-month-long recession period provided a similar value of 330 mm, demonstrating that the stored groundwater is available to sustain streamflow. At the end of the recession, catchment outflow still amounted to 0.9 mm/day with a composite bedrock aquifer providing a disproportionally high share as demonstrated by hydrochemical data. The study demonstrates that high alpine aquifers can seasonally redistribute water and stabilize catchment outflow in an otherwise very dynamic environment and thus might strongly influence the response of such catchments to climate change.

1. Introduction

Mountains are often considered as "water towers" that provide a disproportionally high contribution to river discharge relative to their spatial extent (Viviroli et al., 2007). Mountain ranges can also play an important role in the seasonal redistribution of water. Water is temporary stored as snow or ice and steadily released in warm and dry periods by melt processes hence contributing to the water supply of lowland regions during periods of meteorological drought (Beniston, 2012; Christensen et al., 2004; Rohrer et al., 2013; Sorg et al., 2012). Numerous studies have highlighted that this storage dynamics could be strongly altered in the future by the expected increase in temperature due to climate change (Bales et al., 2006; Baraer et al., 2012; Barnett et al., 2005; Jefferson et al., 2008; Sorg et al., 2012). The disappearance of glacier together with earlier snowmelt and a raising rain/snow line, which has already been documented for several mountainous watersheds, might lead to surface water droughts in summer and late fall (Beniston et al., 2003; Beniston & Stoffel, 2014; Finger et al., 2012; Jefferson et al., 2008; Sorg et al., 2012; Stewart et al., 2004). However, there is considerable uncertainty to what extent groundwater storage in snowmelt dominated systems could dampen this effect by delaying runoff to lowland regions. Thus, there is need for integrated surface and groundwater studies in contrasting geological environments as a foundation for climate impact evaluations.

Compared to lowland areas, there is limited knowledge about the hydrogeological functioning of alpine areas. A key challenge for alpine studies is the stark contrast between the highly heterogeneous nature of such areas versus the usually low data density due to the difficult conditions for monitoring and data acquisition. Direct groundwater observations are often lacking and groundwater storage changes are inferred indirectly. Over the past years, the mechanisms and role of groundwater storage in alpine catchment have been investigated at different scales, reaching from the analysis of larger watersheds to the study of small functional hydrogeological units. Studies at the catchment scales have typically focused on discharge time series and related them to geological and geomorphological features (Jefferson et al., 2008; Lauber et al., 2014). For example, differences in summer low flows and recession behavior in the Cascade Mountains

(Oregon, USA) have been related to differences in groundwater storage as function of the geological age of the volcanic deposits (Tague & Grant, 2004). Modeling studies including some of the same sites suggested that the geological context also influences the catchment response to climate change (Tague & Grant, 2009). However, in these studies, the amount of dynamic groundwater storage was not quantified explicitly. Conceptual hydrological models were used to evaluate the importance of dynamic groundwater storage for sustaining river discharge. In large catchments in the Nepal Himalaya (ranging in size from 32,002 to 57,719 km^2), the estimated dynamic groundwater storage varied between 175 and 310 mm (Andermann et al., 2012). Based on large water table variations observed in a dug well, it was concluded that storage predominately takes place in the fractured basement (Andermann et al., 2012). However, with such models, it is often challenging to separate water storage in form of snow and groundwater. Staudinger et al. (2017) compared four methods (water balance, streamflow recession analysis, conceptual hydrological modeling, and transfer function hydrograph separation model) to evaluate the dynamic storage in 21 alpine and prealpine catchments in Switzerland. They highlighted the significant dynamic storage capacity of high-altitude catchments even with the expected decrease of water storage in form of snow. However, the method comparison also revealed that the estimated storage for a given catchment can vary by up to 1 order of magnitude.

In other studies, geochemical and isotope methods were used to identify the source of water in alpine streams and evaluate the role of groundwater storage (Baraer et al., 2009, 2015; Cowie et al., 2017; Liu et al., 2004; Sueker et al., 2000). The stable isotope composition of water was used to separate a preevent component from event water originating from snowmelt using a two-component mixing model (Klaus & McDonnell, 2013). In addition, chemical tracers were used to separate an unreacted from a reacted component that has traveled through soil or the subsurface (Sueker et al., 2000). Using these approaches, several studies demonstrated that the majority of streamflow in alpine areas often originates from subsurface flow paths. Even at the peak of snowmelt, groundwater can dominate as meltwater infiltrates rapidly and increases hydraulic head gradients in the aquifers (Galleani et al., 2011). For example, Liu et al. (2004) showed that subsurface flow contributes up to 60% of the stream discharge when snowmelt and streamflow discharge reach their peak in an alpine catchment in the Colorado Front Range. However, the hydrograph separation is often associated with a considerable uncertainty as end-members do not have a fixed composition. The stable isotope composition of meltwater evolves during the melt phase (Taylor et al., 2002), and reacted water can have a variable composition depending on the flow path and residence time (Williams et al., 1993).

While such hydrograph-based studies of catchments combined with hydrograph separation provide considerable insight into the contribution of groundwater to streamflow, the mechanism and location of groundwater storage remains uncertain. Several studies have investigated the hydrogeological functioning of small-scale morphological features suspected to be particularly relevant for groundwater storage and quantified storage volumes. In alpine regions, groundwater storage in moraines (Langston et al., 2011; McClymont et al., 2011), alpine meadows, talus complexes (Clow et al., 2003; McClymont et al., 2010; Muir et al., 2011; Roy & Hayashi, 2009), glacier forefields (Gordon et al., 2015; Kobierska et al., 2015), and relict rock glacier (Pauritsch et al., 2017; Winkler et al., 2016) were investigated. A study in the Rocky Mountains suggested that up to >75% of streamflow during storm and winter base flow could originate from talus deposits (Clow et al., 2003). However, a detailed study of a talus structure at another site indicated that storage time scales might be short with recession coefficient as high as 1 day^{-1} (Muir et al., 2011). While such small-scale studies are very valuable to identify storage mechanisms and volumes, it often remains unclear how these hydrogeological units contribute to the larger scale catchment behavior.

An alternative approach to hydrograph-based catchment studies and small-scale process study are investigations in small catchments, where controlling processes can be evaluated and quantified in more detail based on spatially distributed data, while putting them in the context of catchment scale interactions. One of the few studies that quantified dynamic groundwater storage in detail at the catchment scale was carried out at the Opabin site (Yoho National Park, British Columbia, Canada), a 4.7-km^2 large watershed characterized by weathering-resistant quartzite that generates coarse deposits (Hood & Hayashi, 2015). Dynamic groundwater storage was evaluated using a water balance approach. Snow water equivalent (SWE), which is a dominant element of the water balance, was determined by manually measuring the snow height at 1,300 locations. In zones that were inaccessible due to topography and/or exposure to hazards (rock fall and avalanches), the maximum SWE was reconstructed based on the photographically determined date of

snowpack disappearance and a snowmelt model. In the study, the dynamic seasonal groundwater storage (60–100 mm) was related to winter base flow (<0.5 mm/day) highlighting the importance of groundwater storage for the catchment behavior. However, the method is very time consuming and the SWE reconstruction method for winter-inaccessible areas, which are very common in alpine watersheds, introduces additional uncertainty.

The main objectives of this study were therefore to (i) develop and test a rapid methodology to quantify seasonal groundwater storage driven by snowmelt in high alpine catchments, (ii) apply the methodology to an alpine research catchment (Vallon de Réchy, Switzerland), and (iii) investigate the mechanisms of groundwater storage. We quantified the amount of meltwater that is stored beyond the date of complete snowmelt, as it is most relevant to sustain subsequent streamflow in the absence of a snow cover. Because of a highly heterogeneous geological structure, representative water table observations are nearly impossible to acquire in such environments. We accordingly used a water balance approach. We selected the type of acquired data, timing of data acquisition and spatial resolution such as to minimize the uncertainty of the inferred groundwater storage volume. Complementary to the water balance approach, we used hydrochemical methods and $^{3}H/^{3}He$ groundwater dating to discriminate between storage in different hydrogeological units and evaluate how their contribution evolves during a streamflow recession period. Based on the identified main hydrogeological units that store groundwater and by comparison with other sites, we also draw conclusions on conditions that favor high-altitude "suspended" groundwater reserves fed by meltwater.

2. Site Description

The Vallon de Réchy study site consists of an alpine catchment located between 2,150 and 3,148 m above sea level (asl) in the Valais Alps of Switzerland (Figure 1). The catchment covers 11.0 km^2 with a mean altitude of 2,552 m asl. It is located entirely above the tree line and has no glacial cover. Compared to other regions of the Swiss Alps, it receives less precipitation (1,000–1,200 mm/year) due to its position in the inner-alpine zone, surrounded by mountains reaching to 3,500–4,500 m asl.

2.1. Geology and Hydrology

The Vallon de Réchy belongs to the Pennine domain of the Alps. Rock outcrops mainly consist of quartzite, gneiss, and calcschist. In the southeastern part of the catchment (Figure 1), evaporitic rock consisting of gypsum and cargneule (rauhwackes or corgnieule) outcrops can be found (Challandes, 1992). Cargneule originate from alteration of dolomite-bearing evaporites (Schaad, 1995). In this paper, the combination of gypsum and cargneule is denoted as evaporites for simplicity. Dolines are present in this evaporite formation (Figure 1). As a result of major normal east-west faults together with the latter action of glacial erosion, a step-like landscape has been formed consisting of a sequence of rock basins and riegel (Figure 1) as commonly encountered in alpine glacial valleys (Marthaler et al., 2008). On the uppermost plateau, a lake (Lake Louché) is present, while the lower two rock basins were filled with moraine, alluvial deposits and peat forming the Rèche and the Ar du Tsan plateaus (Figure 1). The valley slopes are partly covered by talus deposits, moraine, alluvial fans, and sediments of relict rock glaciers. In the uppermost part of Vallon de Réchy, two active rock glaciers are present. One of them is outside of the watershed and therefore not shown in Figure 1 (Tenthorey, 1993). Furthermore, permafrost tends to occur along the ridges at altitudes above 2,700 m asl (Lugon & Delaloye, 2001). Soil is absent or only very thin.

The stream of the Rèche, originating from Lake Louché drains the watershed and leaves the study area after crossing the riegel of the lowermost rock basin denoted as the Pichioc outlet. This riegel makes it possible to establish a reliable water balance for the entire watershed of Vallon de Réchy. To simplify the reading of this article, we will denote the measuring points as follow in the rest of the article: Lake for Lake Louché, Stream_OUT for Pichioc outlet, Stream_INT for the intermediate station at the Réche plateau, and SO4_Spring for the sulfate-rich spring (Figure 1).

2.2. Difference Between Topographic Basin and Watershed

The watershed is expected to differ from the topographic basin in two zones due to the presence of evaporitic deposits that extent across topographic boundaries. These units act as aquifers with a high drainage capacity

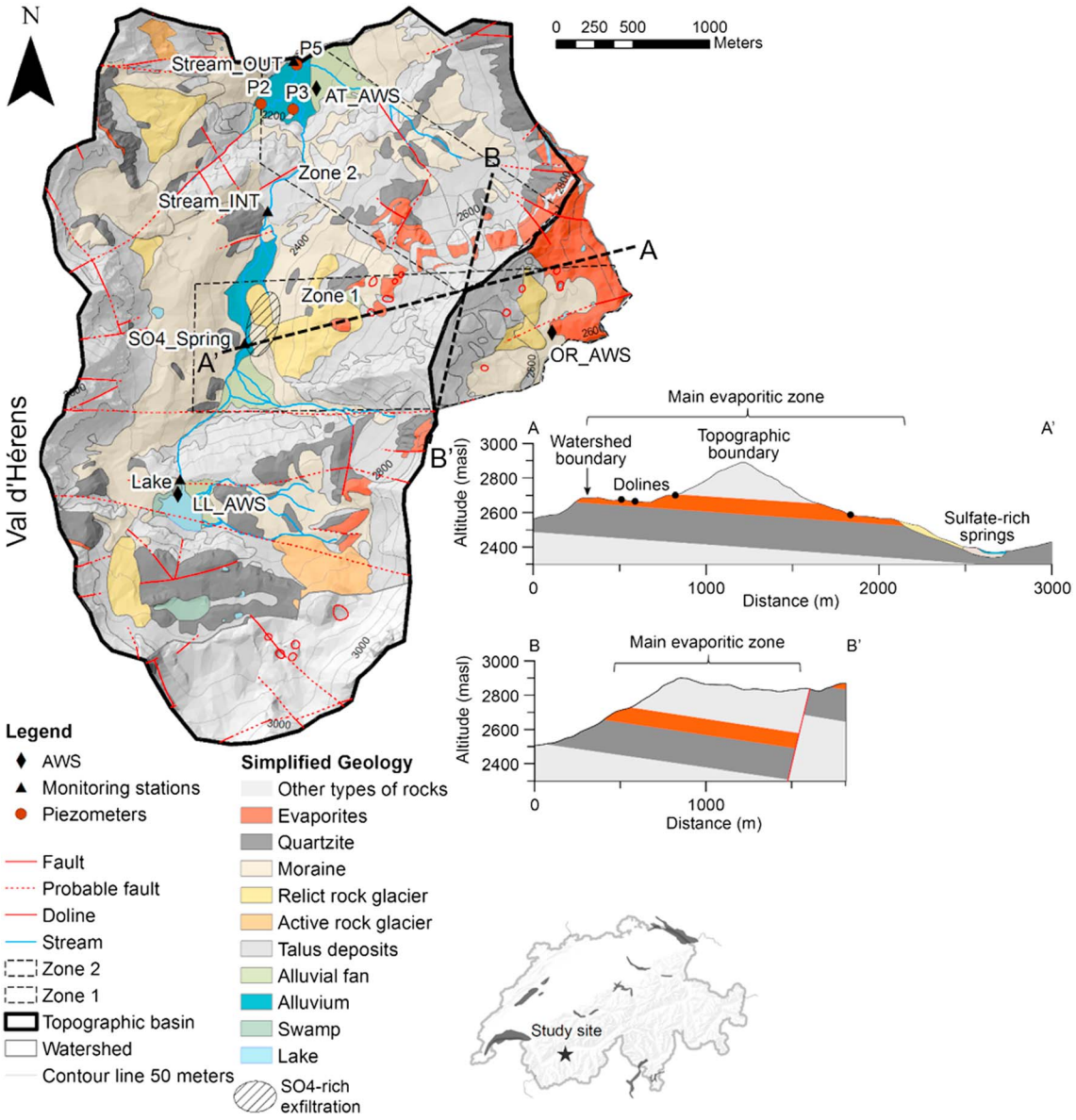

Figure 1. Map and schematic cross sections of the study site (Vallon de Réchy) with simplified geology, location of piezometers (P2, P3, and P5), continuous monitoring stations (Lake, SO4_Spring, Stream_INT and Stream_OUT), and automated weather station (AT_AWS, LL_AWS and OR_AWS). Zones 1 and 2 indicate the areas covered by conceptual models in Figure 7. Simplified geology data and structural feature are based on Swiss Geological Atlas 1:25000/Vissoie (Escher et al., 2008). The topographic shading is based on the digital elevation model swissALTI^{3D} (Wiederkehr & Möri, 2013).

as evidenced by the presence of large dolines, the absence of surface runoff and streamflow where they outcrop, and the presence of large spring systems at their downgradient end. In eastern part of study area, the contact between an extensive evaporitic formation (denoted as main evaporitic zone) and the underlying quartzite dips inward into the valley (dip direction 214 dip angle 07) as illustrated in a schematic cross section (Figure 1). Downgradient of the location where the evaporitic layer reaches its lowest point, a zone with sulfate-rich springs is present (i.e., SO4_spring). For these reasons, the watershed is extended beyond the topographic margin (Figure 1) to include the main evaporitic zone entirely. In the southern part, the opposite occurs, and thus, a portion of the topographic basin is excluded. The absence of sulfate-rich waters in the upper part of the watershed, despite of the presence of large dolines within the topographic basin, confirms that water entering these dolines exits the topographic basin. Previous tracer tests confirmed the connection between the excluded part and zones outside of the topographic basin (Tenthorey, 1993).

3. Materials and Methods

3.1. Methodological Framework

In alpine catchments, groundwater recharge mainly occurs by snowmelt. Thus, to capture the seasonal groundwater storage amplitude, we quantify the groundwater storage increase between the peak of snow accumulation and the moment when snow has completely melted within the catchment. While the storage maximum might be reached before the end of snowmelt (Hood & Hayashi, 2015), storage that persists past the date of complete snowmelt is most relevant for sustaining streamflow in subsequent dry periods. Beyond the period of snowmelt, groundwater is the dominant source of water during dry periods, while before, snowmelt might still contribute to catchment outflow. Furthermore, with this approach, only one detailed SWE survey is required, that is, at the beginning of the main snowmelt period, which reduces the uncertainty of the calculation. For the snowmelt period, the groundwater storage increase corresponds to the following:

$$\Delta S_{GW} = SWE_{MAX} + P - R - E - S - A \quad (1)$$

with

ΔS_{GW}	dynamic groundwater storage
SWE_{max}	SWE at the beginning of the main snowmelt period
P	precipitation
R	runoff from the catchment
E	evapotranspiration
S	sublimation
A	water abstraction for drinking water supply

As soils are absent or only very thin, we neglected changes in soil water storage. Furthermore, the volume change of Lake Louché is insignificant at the catchment scale. The active rock glacier within the watershed is not expected to influence the water balance, as it only covers 1.5% of the watershed surface.

Due to the short time period over which the water balance is evaluated and the strong influence of snow, two terms dominate the water balance, SWE_{max} and R, while precipitation, evapotranspiration, and sublimation are comparatively small, and thus, uncertainties associated with these terms have a minor effect on the calculated groundwater storage. While for R, standard procedures (i.e., rating curves) provide sufficiently accurate data, the accuracy of the calculated dynamic groundwater storage crucially depends on the method to quantify SWE_{max}, the largest term in the equation. For accurate SWE quantification, accurate snow height data are particularly important as snow height varies over a larger range than snow density (Jonas et al., 2009). A key element of the proposed methodology is the use airborne LIDAR technology to overcome the limited accessibility of high-altitude catchments, and to obtain accurate snow height data at a very high spatial resolution.

To verify the plausibility of the calculated groundwater storage increase, we also calculate the subsequent seasonal groundwater storage depletion. The two terms should agree approximately although interannual changes in groundwater storage can led to discrepancies. We quantify storage depletion for two phases, the phase between the end of snowmelt and the beginning of snow accumulation (snow-free period) using the following:

$$\Delta S_{GW} = P - R - E - A \quad (2)$$

and for the winter phase, recession period until the onset of snowmelt using the following:

$$\Delta S_{GW} = -R - A \quad (3)$$

During the latter period, precipitation accumulates mostly in form of snow. Only a small part of precipitation falls in form of rain at the beginning of the winter period (e.g., first week of November). We quantify the uncertainty of the calculated storage volumes from the uncertainties of the various terms of the water balance using standard uncertainty propagation laws.

Table 1
Overview of Meteorological and Hydrological Parameters That Were Recorded Continuously From December 2012 to July 2014

Location	Parameter	Manufacturer	Model	Uncertainty
Ar du Tsan automatic weather station AT_AWS	Air temperature	Sensirion, Stäfa, Switzerland	SHT75	±0.3 °C
	Humidity			±1.8 %RH
	Precipitation[a]	Ott Hydrometrie, Mellingen, Germany	OTT Pluvio2	± 0.1 mm
	Precipitation[b]			±4%
	Solar radiation	Davis, Hayward, CA, USA	Vantage Pro	±90 W/m
	Wind speed			±5%
	Wind direction			±7°
	Snow height	Campbell	SR50A	±1 cm
Lake Louché automatic weather station LL_AWS	Precipitation	Ott Hydrometrie, Mellingen, Germany	OTT Pluvio2	±0.1 mm
Stream_OUT	Stream stage	MADD, Yverdon-les-Bains, Switzerland	HyMADD	±10 mm
	Temperature			±0.2 °C
	Electrical conductivity			±40 μS/cm
Lake Stream_INT SO4_Spring	Temperature	Onset, Bourne, WA, USA	U24 Freshwater Conductivity Data Logger	±0.3 °C
	Electrical conductivity			±3%
Piezometers P2, P3, and P5	Groundwater level	Keller, Winterthur, Switzerland	DCX-16	±10 mm
Mont Noble	Still image	Campell, Logan, UT, USA	CC5MPX	na

Note. Manufacturer and model of the used instrument. Uncertainty as specified by the manufacturer. The measurement location are indicated in Figure 1. na = not applicable.
[a]From April 2014. [b]Until April 2014.

To differentiate among groundwater storage locations; we also evaluate the hydrochemical composition of groundwater and surface water. For bedrock, groundwater storage is expected to occur in the more permeable evaporitic rock. In this unit, groundwater should acquire a hydrochemical signature that differs from groundwater stored in the unconsolidated deposits. Furthermore, we evaluate groundwater table fluctuations at locations in the catchment with easier access (P2, P3, and P5 in Figure 1) to obtain qualitative information on the groundwater storage dynamics, although these data are not sufficiently representative for the entire catchment to calculate water balances.

3.2. Data Acquisition

We acquired field data for this study from December 2012 to July 2014 to evaluate the catchment behavior during a full snow accumulation, melt and recession cycle. We recorded various meteorological and hydrological parameters continuously as summarized in Table 1. In addition, we sampled stream water and groundwater to characterize its hydrochemical composition. In the following, the measurement and sampling locations (Figure 1) and the methods are described in more detail.

3.2.1. Meteorological Measurement

We recorded meteorological parameters (Table 1) every minute at the Ar du Tsan plateau automatic weather station (AT_AWS) at 2,193 m asl (Figure 1). In order to estimate the altitudinal precipitation gradient, we installed a second weather station in autumn 2014 at Lake Louché (LL_AWS, 2,567 m asl). We corrected liquid precipitation data for wind undercatch and wetting losses, while evaporation and splash-in splash-out losses were assumed to be negligible (Dingman, 2015; World Meteorological Organization, WMO, 2008). As the correlation coefficient between precipitation and wind speed was 0.03, we estimated wind undercatch using the mean wind speed (1.3 m/s) at the Ar du Tsan plateau and obtained a correction factor of 1.03 or 3% (Larson & Peck, 1974; WMO, 2008). Wetting losses were estimated at 3% (Sevruk, 1974; WMO, 2008). We measured solid precipitation only from April 2014 at AT_AWS when a suitable device was installed (Table 1). Before April 2014, we used data from the Evolène/Villa (EVO) Meteoswiss AWS (1,825 m asl) located 10 km away from AT_AWS.

3.2.2. Snowpack Measurement

We recorded the snow height continuously at the AT_AWS (2,193 m asl). In addition, we obtained snow height data for OR_AWS (2,630 m asl) from the Swiss institute for snow and avalanche research. At the peak of snow accumulation, the snow height was mapped by the company Helimap using airborne LIDAR as

described in Sovilla et al. (2010), but with more advanced instruments that further reduced uncertainty. The uncertainty of LIDAR is influenced by several factors including errors in the positioning, the attitude (i.e., orientation of the aircraft), and errors of the laser itself (Glennie, 2007). A particularity of measurements in alpine area is that the measurement range and incidence angle vary considerably due to topography. This requires that angular uncertainties are particularly well constrained as they lead to larger offsets for longer range and sloped terrain. Angular uncertainties can originate from the inertial measurement unit (IMU) used to determine the aircraft attitude and from the laser itself as a function of its angular resolution and beam divergence (Glennie, 2007). Furthermore, long-range measurements can lead to multiple pulse in air effects, which complicate the allocation of return pulses to specific transmissions.

The utilized equipment, consisting of a RIEGL VQ580 with an iXblue Airins IMU and dual-frequency GPS receiver, is particularly well suited to deal with these challenges. The iXblue Airins IMU has a low uncertainty for row (0.002°), pitch (0.002°), and heading (0.006°). The RIEGL VG580, specifically designed to measure snow and ice, has a low range uncertainty (25 mm), a high angular resolution (0.001°), and a narrow laser beam (0.2 mrad). It is capable of uniquely attributing multiple pulses in air thus ensuring precise and robust range measurements irrespectively of distance (Riegl, 2015). Its wavelength of 1,064 nm is well suited to characterize snow surfaces as most of the reflected signal comes from the top 1 cm (Deems et al., 2013).

Data were acquired at a rate of 10,000 points per second. The measurements were related to the national coordinate frame using a GPS reference station and were mapped onto a Cartesian grid with 0.5-m spacing. The heights were interpolated at each vertex and a moving average of 10 × 10 cells was applied to reduce local errors. Negative values relative to the ground surface were set to zero and missing values were interpolated using nearest neighbor interpolation. The estimated absolute accuracies for the position is 5–7 cm in Z direction and 10 cm in X and Y directions. The LIDAR survey covered 91% of the watershed; the remaining 9% was estimated based on the mean snow height measured at the same altitude at locations within the measurement area.

On the day of the LIDAR survey (5 June 2013), we determined the profile-averaged snow density at 10 locations between 2,500 and 2,950 m asl. We measured snow density on site using a snow density gauge (Adirondack Type, P5000-0000, GENEQ). We installed a camera CC5MPX (Campbell Scientific) on Mont Noble (2,640 m asl) on the eastern ridge of the watershed to monitor the evolution of the snow cover and confirm the timing of complete snowmelt, which occurred at the end of July 2013.

3.2.3. Continuous Monitoring of Streamflow, Temperature, and Electrical Conductivity

We recorded stream stage, temperature, and electrical conductivity (EC) continuously at Stream_OUT (Figure 1). To establish a rating curve, we measured the discharge of the Rèche during 15 campaigns using the salt dilution method covering a wide range of discharge values, from 100 to 1,250 L/s. In addition to Stream_OUT, we recorded EC and temperature also at Lake, Stream_INT and at SO4_Spring (Figure 1 and Table 1). We transformed EC values to a reference temperature of 25 °C.

3.2.4. Groundwater Levels

We installed six piezometers reaching from 2.2- to 4.4-m depth in the alluvial plain of Ar du Tsan to record groundwater levels (Figure 1). The piezometers consist of screened polyvinyl chloride tubes (2.54-cm diameter) surrounded by a gravel pack. Three of the six piezometers (P2, P3, and P5, Figures 1 and 2) were equipped with pressure sensors (Table 1).

3.2.5. Water Sampling

We sampled stream water and groundwater to measure the dissolved sulfate concentration, EC and temperature. We measured EC and temperature using a WTW ProfiLine Cond 3310. We filtered samples, stored them in high-density polyethylene bottles and analyzed them by ion chromatography (Dionex DX-120).

3.2.6. Groundwater Dating

We determined the age of groundwater from the SO4_Spring using the $^{3}H/^{3}He$ method. We collected water samples for dissolved noble gas (^{3}He, ^{4}He, and ^{20}Ne) and ^{3}H in copper tubes (Beyerle et al., 2000) and a glass bottle, respectively on 21 October 2014. The noble gases were analyzed by mass spectrometry (Sultenfuss et al., 2009) with an analytical uncertainty of 1%. Tritium was electrolytically enriched and measured by liquid scintillation counting by Hydroisotop GmbH (Germany) with an uncertainty of 1 TU (tritium unit). As Ne has only an atmospheric source, we used offsets between measured and solubility equilibrium concentrations of Ne, expressed as ΔNe, as a proxy for excess air. We calculated the terrigenic He component as the

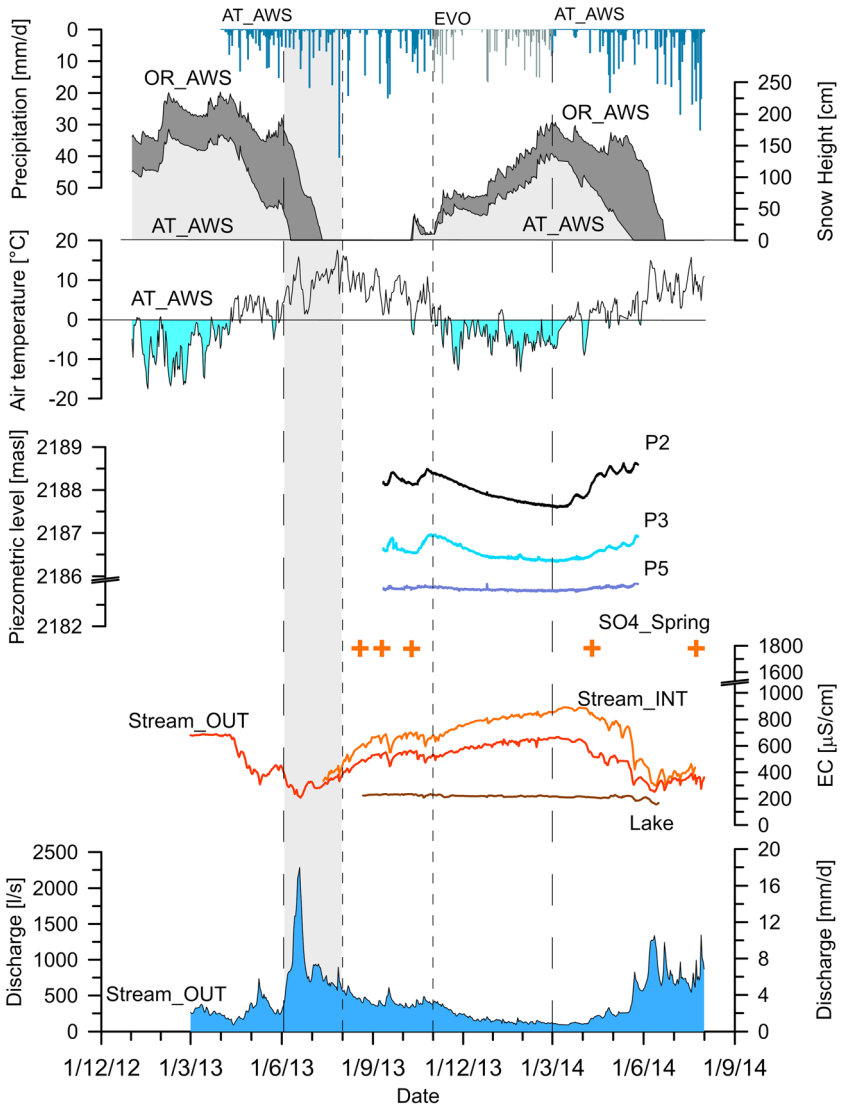

Figure 2. Time series of meteorological, hydrological, and hydrochemical parameters. The main melt period for 2013 is highlighted in gray. The name refers to piezometers (P2, P3, and P5), continuous monitoring stations (Lake, SO4_Spring, Stream_INT and Stream_OUT), automated weather station (AT_AWS, LL_AWS, and OR_AWS) and Meteosuisse automatic weather station (EVO). EC = electrical conductivity.

measured concentration minus the equilibrium and excess air components, assuming a terrigenic $^{3}He/^{4}He$ ratio of $1 * 10^{-8}$. We calculated the tritiogenic He (^{3}He) by deducing the estimated solubility equilibrium, excess air, and terrigenic components from measured ^{3}He concentrations.

3.3. Quantification of Water Balance Terms and Their Associated Uncertainties

3.3.1. Precipitation

For the water balance calculations, precipitation is only quantified for the period between the peak of snow accumulation until the beginning of the subsequent period of snow accumulation in early winter. During this period, most of the precipitation falls in the form of rain, which can be measured with a lower uncertainty than snowfall. Based on the two weather stations within the watershed (AT_AWS and LL_AWS), we quantified the altitude gradient of precipitation (4.1%/100 m). This altitude gradient is in good agreement with values from other sites in the Swiss Alps (Sevruk, 1997). We used the altitude gradient to extrapolate precipitation data from the AT_AWS to the entire catchment using a digital terrain model.

3.3.2. SWE

The snow volume corresponds to the difference between the snow surface and land surface recorded by LIDAR and mapped on a 0.5-m grid. We calculated the SWE by multiplying the snow volume with the average snow density. We quantified the uncertainty of the snow volume according to the method developed by Hartzell et al. (2015). The variance of the snow volume is as follows:

$$\sigma^2_{\mathrm{SV}} = A^2_{\mathrm{rc}} \left(\sum_{i=1}^{n} \sigma^2_{\mathrm{ES},i} + \sum_{i=1}^{n} \sigma^2_{\mathrm{EG},i} \right) \tag{4}$$

With

A^2_{rc}	Raster cell area (L^2)
σ^2_{SV}	variance of snow volume
$\sigma^2_{EG,i}$	variance of ground surface elevation
$\sigma^2_{ES,i}$	variance of snow surface elevation
n	number of grid cells

The right-hand side of the equation incorporates the uncertainty of the ground surface and snow elevation. We quantified the uncertainty of the mean snow density from the measured ground-based snow density measurements. We then quantified the uncertainty of the SWE by error propagation from the uncertainties of the snow volume and the snow density.

For comparison, we also determined the SWE using a published, empirical relationship between snow density, season, snow height, and altitude to represent a situation where ground-based snow density measurements might not be available, for example, due to inaccessibility of the site. The relationship had been derived from 11,147 data record from 48 winters and 37 stations throughout the Alps (Jonas et al., 2009).

3.3.3. Sublimation

Sublimation in alpine areas varies depending on the topography and climate. Typical values for similar alpine sites are 10% SWE (DeWalle & Rango, 2008; Strasser et al., 2008). According to Hood et al. (1999), sublimation occurs mainly during the snow accumulation season and becomes less significant during the snowmelt period. During the melt period, condensation on the remaining snow pack rather than sublimation can occur. As we calculate the water balance for a short period between peak of snow accumulation and date of complete snowmelt, we consider sublimation not to be significant. If condensation rather than sublimation would occur, the groundwater storage increase would be underestimated when sublimation/condensation is neglected.

3.3.4. Runoff

We quantified the surface runoff at the catchment outlet (Stream_OUT) by integrating the continuous discharge time series over time. Uncertainties associated with streamflow estimation are as follows: uncertainty of water depth using a MADD probe of 0.5%, uncertainty of salt gauging method of 5% (Moore, 2004), and uncertainty of the rating curve of 10%. Given that these uncertainties are uncorrelated, the total uncertainty was calculated using the root mean square propagation method (Harmel et al., 2006) and a value of 11% was obtained.

3.3.5. Evapotranspiration

We calculated potential evapotranspiration, $P_E\,(m/d)$ from vegetated areas using the equation from Priestley and Taylor (1972):

$$P_E = \alpha \frac{\Delta}{\Delta + \gamma} \frac{\mathrm{R_n} - \mathrm{G}}{L\,\rho_w} \tag{5}$$

where α is a dimensionless parameter, Δ (kPa/°C) is the slope of vapor pressure curve, γ (kPa/°C) is the psychometric constant, R_n (MJ/m^2/day) is the net radiation, G (MJ/m^2/day) is soil heat flux, L (MJ/kg) is the latent heat of vaporization, and ρ_w the density of water (kg/m^3). We estimated R_n according to Allen et al. (1998), parameters not measured at AT_AWS were estimated from the measurement done at Meteoswiss Evolène/Villa (EVO) weather station. P_E was calculated on a daily basis; therefore, G was assumed to be negligible (Allen et al., 1998). For the alpine environment, $\alpha = 1$ was used as suggested by various authors (Eaton et al., 2001; Hood & Hayashi, 2015; Saunders et al., 1997). Evapotranspiration from nonvegetated area such

as talus areas and bedrock is assumed to be negligible. The uncertainty of evapotranspiration was estimated to be 20%, based on error propagation similarly to Nichols et al. (2004).

4. Results and Discussion

4.1. Meteorological, Hydrological, and Hydrochemical Parameters

In winter 2012/2013, temperatures stayed below the freezing point for most of the period between 20 November 2012 and 13 April 2013 at the AT_AWS (2,193 m asl) and up to 160 cm of snow accumulated (Figure 2). At the higher-altitude Orzival station (OR_AWS, 2,620 m asl), more snow (up to 232 cm) accumulated. Some snowmelt occurred in April 2013 interrupted by another period with subzero temperatures in May 2013. The main snowmelt period started at the beginning of June and the snow cover had completely disappeared in the entire catchment by 31 July 2013. Concurrent with the two melt phases, two periods with elevated discharge can be observed at Stream_OUT (Figure 2), with a much larger increase during the main melt period. After the end of snowmelt, the hydrograph is characterized by a long recession period extending until the beginning of April 2014 with a minimal discharge of 120 L/s (=0.9 mm/day).

In summer 2013, Stream_INT showed only limited reaction to rainfall events. The baseflow as determined by the local minimum method was always higher than the superimposed discharge peaks. Moreover, a more humid period from mid-October to mid-November 2013 leads to an overall baseflow increase rather than a series of discernable discharge peaks. The small reaction of the catchment to rain events reflects the high infiltration capacity of the watershed.

Groundwater levels steadily decreased during the winter recession period in P2 and P3, while it remained relatively stable in P5 (Figure 2). The different behavior is related to the location of the piezometers. P5 is located at the downgradient end of the Ar du Tsan plateau close to Stream_OUT (Figure 1) where groundwater discharge likely occurs. Hence, the water table is controlled by the stream level. P2 and P3 are further up gradient and the water table position reflects the balance between groundwater recharge and flow toward the discharge zone. Rain events in summer and snowmelt lead to an increase of the water table while during the period with snow cover, groundwater levels steadily decrease over several months.

4.2. Hydrochemical Parameters

The EC remained stable in the SO4_spring and in Lake, except for a small decrease during the melt period at Lake (Figure 2). In contrast, EC varied by 520 and 370 μs/cm at Stream_OUT and Stream_INT, respectively, dropping rapidly at the onset of snowmelt and then slowly recovering again during the recession period (Figure 2). The EC always increased from Lake toward Stream_INT and then decreased again until Stream_OUT. Thus, highly mineralized water reached the Rèche between Lake and Stream_INT and was then diluted again by less mineralized water between Stream_INT and Stream_OUT. The EC increase occurs in the central part of the valley, where an extensive layer of evaporitic rock dips inward into the valley (Figure 1). This layer likely hosts a deeper groundwater flow system and is the source of the highly mineralized water. Indeed, when plotting the EC against sulfate concentrations, a strong correlation can be observed (Figure S1 in the supporting information). The highest sulfate concentration was measured in the SO_4 spring. For this location, a saturation index with respect of Gypsum of -0.21 ± 0.03 is obtained indicating that the sample is close to equilibrium with the mineral. The $^3H/^3He$ age of water from the SO4_spring was 11.1 years providing further evidence for a deeper groundwater flow system through the main evaporitic unit.

4.3. Quantification of SWE

The snow height on 5 June 2013 is illustrated for 20-m elevation bands (Figure 3) together with the values from AT_AWS and OR_AWS, which are located at sites with a small tendency for snow redistribution. The snow height generally increases with altitude as expected due to the higher precipitation with altitude and some snowmelt at lower altitude before the LIDAR campaign. The mean snow height obtained by LIDAR agrees well with the point measurements at AT_AWS and OR_AWS. The mean measured snow density was 450 ± 60 kg/m^3. For the entire watershed, the SWE was 660 ± 32 mm or $7{,}290{,}000 \pm 360{,}000$ m^3. The mean snow density calculated according to statistical method of Jonas et al. (2009) is 460 kg/m^3, which is within the range of uncertainty of the ground-based measurements. Using the calculated snow density, a

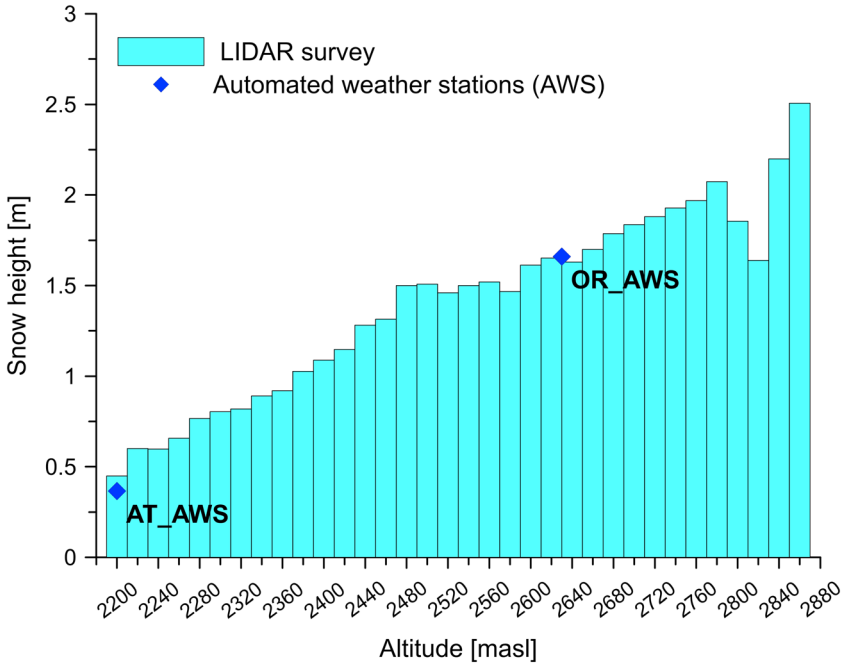

Figure 3. Altitudinal evolution of snow height measured with the LIDAR survey on 5 June 2013. Every bar represent the mean snow height for the 20-m altitude class. The diamonds represent the snow height measured at AT_AWS and OR_AWS the day of the LIDAR survey.

watershed SWE of 680 mm or 7,500,000 m^3 is obtained, which is within range of uncertainty of the value obtained based on measured snow densities.

4.4. Quantification of Dynamic Groundwater Storage

We quantified the groundwater storage increase for the main snowmelt period between 5 June and 31 July 2013 with the former date corresponding to the day of the detailed LIDAR snow mapping campaign and the latter to moment when the snow cover had completely vanished. We divided the recession period into two parts: a first one until initiation of new snow accumulation (snow-free period) and a second one until the onset of snowmelt (snow accumulation period).

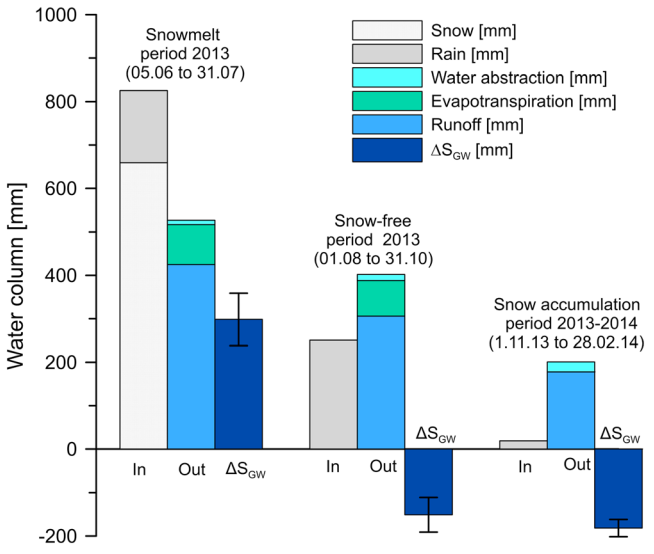

Figure 4. Water balance for different periods of the year (snowmelt period, snow-free period, and snow accumulation period) between the 5 June 2013 and 28 February 2014. Error bar represent the uncertainty associated with ΔS_{GW} estimation.

In the snowmelt period, catchment outflow via the creek and water abstraction corresponded only to about half of the input of water from snowmelt and rain (Figure 4). If the estimated evapotranspiration is considered as well, an increase of groundwater storage by 300 ± 60 mm (or 5.3 mm/day) is obtained, corresponding to 45% of the premelt SWE or 36% of the premelt SWE plus precipitation during the snowmelt period. If the calculated snow density according to Jonas et al., 2009 is used rather than the measured one, the calculated groundwater storage amounts to 322 mm, which is within the range of uncertainty of the value obtained based on direct snow density measurements. Thus, dynamic groundwater storage can be quantified reliably even without manual ground-based measurements adding to the practical viability of the method.

During the snow-free period, the catchment outflow (creek and water abstraction) is larger than the total precipitation (Figure 4). Considering evapotranspiration, the storage loss amounts to 150 ± 40 mm (or 1.7 mm/day). In the snow accumulation period, the groundwater storage loss is 180 mm ± 20 mm (or 1.5 mm/day). Overall, groundwater storage depletion amounts to 330 mm over a period of 7 months. The

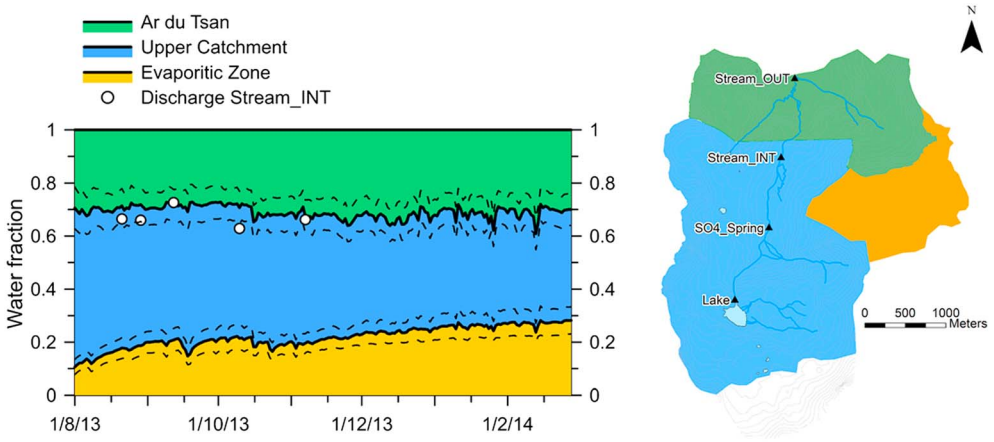

Figure 5. Contribution of three zones of the catchment to outflow during recession period and fraction originating from evaporitic zone. The white points represent punctual discharge measurements at Stream_INT.

independently calculated storage increase (300 ± 60 mm) and loss (330 ± 45 mm) agree well and are associated with a similar uncertainty. The good agreement between the two quantities and the relatively small uncertainties demonstrate (1) that the groundwater dynamics can be quantified reliably with the proposed methodology despite of the complexity of high alpine catchments and (2) that water is indeed stored as groundwater available to subsequently sustain streamflow and not as, for example, soil moisture that is evapotranspirated again. The calculated groundwater storage increase shows only a small sensitivity to the uncertainty of less well constrained terms of the water balance, especially evapotranspiration. If evapotranspiration were to be 50% higher or lower than estimated, the calculated groundwater storage would only change by 14%. If the data of the LIDAR campaign do not match exactly the peak of snow accumulation, groundwater storage is underestimated because either some snow has not fallen yet or part of it has already melted.

4.5. Hydrograph Separation

To gain additional insight into locations and mechanisms of groundwater storage, we evaluated the EC data in more detail and performed a hydrograph separation for the recession period. EC can be considered as a proxy for sulfate (see high correlation in Figure S1), with the advantage that it can be measured continuously. Sulfate is expected to show a conservative behavior as the streams are under oxic conditions, preventing sulfate reduction to occur, sulfate has a very low tendency to participate in ion exchange or surface complexation (Langmuir, 1997) and mixing of waters does not provoke its precipitation. While in classical hydrograph separation, the respective contributions of different water types (precipitation, soil water, and groundwater) are differentiated, we partitioned the catchment outflow according to its provenance in the watershed. In particular, we aimed at quantifying the contribution from the deeper aquifer in the evaporitic zone. Based on the collected EC data, we separated the Vallon de Réchy in three zones as illustrated in Figure 5: the Ar du Tsan plateau (lower catchment), the main evaporitic zone with a distinctive groundwater signature, and the higher Rèche-Lake Louché domain (upper catchment). We delineated the main evaporitic zone based on its outcrops on the northern, eastern, and western edge and a major fault on the southern side (Figure 1). The lower catchment corresponds to lowest basin created by a major fault (see section 2.1), the upper catchment to the zone upgradient of it. We quantified the contributions of these three zones by two sequential hydrograph separations each separating two components. We calculated the fraction of water coming from the Ar du Tsan zone, f_{AT}, as follows:

$$f_{AT} = \frac{EC_{INT} - EC_{OUT}}{EC_{INT} - EC_{AT}} \quad (6)$$

based on EC of water flowing into this zone measured at Stream_INT (EC_{INT}), water leaving the zone at Stream_OUT (EC_{OUT}) and water from the lower catchment (EC_{AT}). While the former two values have been measured continuously, we defined the latter based on manual measurement of the EC of small springs and

lower order creeks in the Ar du Tsan Zone section, which varied between 180 and 240 μS/cm. This range of values is consistent with the absence of evaporitic rock, except for a small patch in the eastern most section. For the calculation, we used the average value of 210 ± 15 μS/cm for EC_{AT}.

The fraction of water originating from the evaporitic zone, f_{EZ}, corresponds to the following:

$$f_{EZ} = (1-f_{AT}) \cdot \frac{EC_{INT}-EC_{UC}}{EC_{EZ}-EC_{UC}} \quad (7)$$

where EC_{UC} is the electrical conductivity of water from the upper catchment and EC_{EZ} is the electrical conductivity of groundwater from the deeper evaporitic aquifer. Except for the evaporitic zone, water in the upper catchment has a similar composition as in the Ar du Tsan section due to the similarity of the geological and geochemical conditions. For this section, we used the average EC of the outflow of Lake during the recession period (190 μS/cm), which averages over a large area. We assumed that groundwater transiting through the main evaporitic zone is in equilibrium with gypsum as this mineral dissolves rapidly (Lebedev, 2015) and the residence time in the aquifer is long as shown by the $^3H/^3He$ dating. Therefore, we used the average EC of SO4_spring for EC_{EZ}. Although the two other zones also show occurrence of evaporitic rock (Figure 1), it does not influence the water chemistry as indicated by the EC of water downgradient of these zones, which range between 180 and 240 μS/cm (Arc du Tsan) and 190 uS/cm (Lake Louché). Discrete discharge measurements at Stream_INT, which is the sum of the upper catchment and the evaporitic zone discharge, are in good agreement with the results of the hydrograph separation (Figure 5) confirming the validity of the approach.

During the recession period, the contributions of different zones to the stream discharge shifted. The contribution of the main evaporitic zone increased from about 10% to 30%, the contribution of the upper catchment decreased from 60% to 40% while the contribution of the Ar du Tsan zone remained stable. Although the main evaporitic zone covers only 15% of the catchment area, it contributed a disproportionally high amount of 30% of discharge at the end of the recession period. While the relative contributions of the three zones are similar at the end of the recession period (30–40%), large differences in the capacity to yield water become apparent if the respective areas are taken into account. At the end of recession period, the specific discharge amounts to 1.6 mm/day (18 L/s/km^2) for the main evaporitic zone, 1.0 mm/day (11 L/s/km^2) for the Ar de Tsan zone and 0.6 mm/day (7 L/s/km^2) for the upper catchment.

4.6. Mechanism of Groundwater Storage

The study demonstrates that high alpine catchments have the ability to store a substantial quantity of groundwater and ensure a stable catchment outflow over months. This is contrary to the intuition that in steep catchments, water drains out quickly. In the following, the reasons for the high water storage potential are discussed. At the study site, the deeper evaporitic rock layer contributes to groundwater storage although it is somewhat counterintuitive that one of the steepest and highest-altitude zones in the catchment provides a disproportionally high contribution to winter baseflow. The functioning of this zone is illustrated in a conceptual diagram (Figure 6a). The groundwater storage potential is in this case not controlled by the surface topography but rather the geometry of the contact between this layer and the underlying less permeable quartzite. This interface only gently dips (7°), thus helping to retain groundwater. Groundwater storage is further favored by a major normal fault (Figure 1) that brings the upvalley end of the evaporitic layer in contact with a less permeable rock. The presence of dolines in the evaporitic zone on either side of the ridge (Figure 1) and the absence of surface flow features confirm that most water infiltrates into the subsurface. In the evaporitic layer, groundwater flows in opposite direction to the valley gradient as evidenced by the position of the sources with sulfate-rich water in the most upvalley part of the evaporitic unit. The sulfate-rich water likely reaches the springs via a relict rock glacier and moraines. These observations demonstrate that the "subsurface topography" can strongly influence the drainage behavior of a catchment, which might be overlooked by classical catchment mapping methods that focus on the surface topography and geomorphology. While the hydrograph separation suggests that different zones of the catchment act in parallel to influence the recession behavior, we hypothesize that the sequential coupling of geological elements capable of storing or transmitting water might play an important role as well. However, we have not quantified such exchange mechanisms. Thus, they remain hypothetical and are meant to simulate future research. At our site, massive accumulations of talus deposits are located on top of the evaporitic unit. These materials

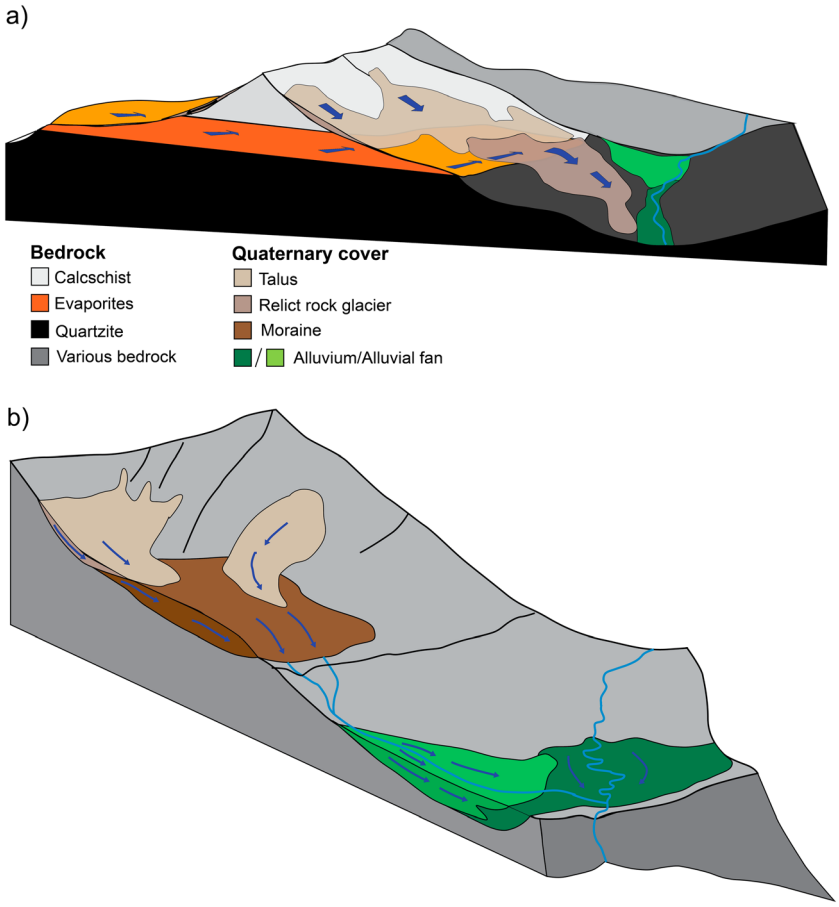

Figure 6. (a) Conceptual scheme of interacting flow and storage processes involving a bedrock aquifer in the central part of the catchment (Zone 1, Figure 1) and (b) different type of quaternary deposits in the lower Ar du Tsan part (Zone 2, Figure 1).

might act as a porous aquifer that collects rain and meltwater, stores it for an initial period, and then transmits it to the underlying evaporitic unit where storage takes place again. Such sequential storage might also explain why the lower catchment (Ar du Tsan plateau) is characterized by an above average discharge rate at the end of the winter recession period (Figure 6b). In this part, there is no direct evidence for storage of water in deeper bedrock. In this zone, water can potentially pass through talus deposit to moraine, exfiltrate from the moraine where the quartzite formation outcrops, then reinfiltrate in an alluvial fan that is intertwined with the alluvial deposits of the Rèche. Hence, an assemblage of permeable units in sequence and parallel as encountered in our study site with a high geological complexity may favor water retention and lead to a slow recession.

4.7. Comparison With Other Sites

There are only few other high alpine watersheds for which dynamic groundwater storage was quantified at a similar precision, among them the Opabin watershed. The dynamic groundwater storage measured at the Vallon de Réchy is considerably higher than that at the Opabin watershed. In the Vallon de Réchy, it amounted to 300 mm for a premelt SWE of 660 mm or 45%, whereas at Opabin 60–100 mm were stored for a premelt SWE of 500–640 mm or 9–20% (Hood & Hayashi, 2015). The same applies for the stream discharge at the end of the recession period, with a value for Vallon de Réchy of 0.9 mm/day compared to 0.5 mm/day at the Opabin watershed. The differences in groundwater storage among the two sites can be related to their geology. The Opabin site is located in quartzite lithology, which is resistant to weathering and erosion, and produces coarse deposits. Hence, groundwater storage in the bedrock is not relevant and groundwater storage time scales are likely shorter in the coarser unconsolidated deposits. In contrast, at the Réchy site, substantial groundwater storage occurs in the bedrock and the unconsolidated material

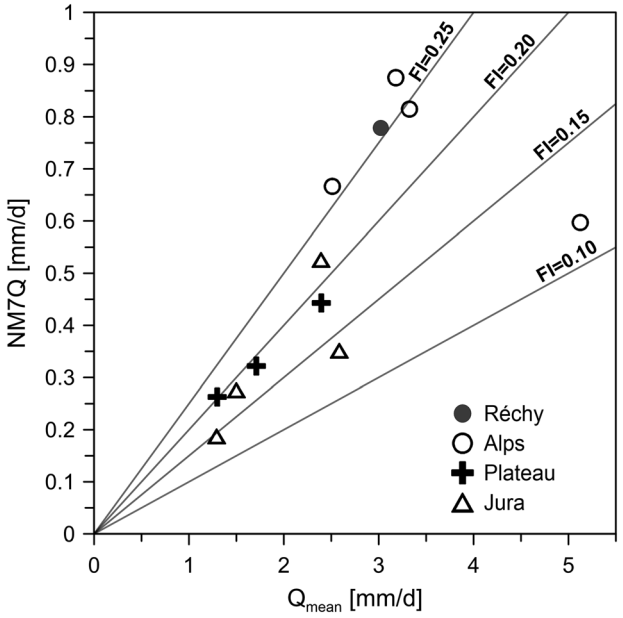

Figure 7. Flow index (FI) is the ratio between the minimum mean discharge over seven days and the mean annual discharge (FI = NM7Q/Q_{mean}). Details on the catchment characteristics can be found in Table S1.

partly originating from lithologies that weather more easily and thus are expected to have a lower hydraulic conductivity. The obtained dynamic groundwater storage values for Vallon de Réchy (300–330 mm) are in a similar range to the highest values obtained for much bigger catchments in the Nepal Himalaya (up to 310 mm for large catchments, up to 440 mm for smaller catchments) using conceptual hydrological models (Andermann et al., 2012). Similarly as at our site, groundwater storage in the different cohesive rock formations ("composite bedrock") was also hypothesized as an important factor contributing to the high dynamic groundwater storage. Other studies have also highlighted the importance of permeable bedrock for groundwater storage for a wide range of lithologies such as volcanic rock (Tague & Grant, 2004), permeable sedimentary rock (Carlier et al., 2018; Pfister et al., 2017; Sayama et al., 2011), or weather crystalline rock (Katsuyama et al., 2005). Some authors have demonstrated that, in presence of a permeable bedrock, steeper catchment can store more water (Sayama et al., 2011), highlighting the importance of mountainous areas for their capacity to effectively store water. This seemingly contradictory finding was rationalized by the larger volume available for groundwater storage and release, denoted as the active bedrock hypothesis (Sayama et al., 2011; Uchida et al., 2008). However, these studies did not consider the often complex geometry of the interface with underlying lower permeability units, which becomes highly relevant in the case of tectonized alpine bedrock aquifers.

To place this study in a broader context, we also compared the results from Vallon de Réchy site to other alpine and lowland watershed in Switzerland. As for the other watershed data to quantify dynamic groundwater storage with similar accuracy are lacking, two related metrics were compared, that is, discharge rates at the end of long recession periods, and for other alpine catchments, catchment outflow during the winter recession period. We quantified the catchment outflow after prolonged recession periods based on the NM7Q low flow indicator, which is the minimum discharge over seven consecutive days (Haller et al., 2004). We averaged these indicators for a period of 20 years from 1991 to 2010. For the Vallon de Rechy, we processed discharge data measured at the outlet to calculate NM7Q for the period from the 1 April 2013 to the 31 March 2014. In order to compare low flow data without a climatic bias (Paznekas & Hayashi, 2016), we calculated a flow index (FI) according to previous studies (Burn et al., 2008; Paznekas & Hayashi, 2016) by normalizing the low flow discharge by the mean discharge (equation 8).

$$\mathrm{FI} = Q_{\mathrm{NM7Q}}/Q_{\mathrm{Mean}} \tag{8}$$

where Q_{NM7Q} is the minimum discharge over seven consecutive days and Q_{Mean} is the mean discharge.

We classified the selected catchments from the NQstat database (Federal Office of the Environment, 2011) according to main geologic and geographic areas of Switzerland (Jura, Plateau, and Alps). Three of the four alpine catchments have a FI similar to the Vallon de Réchy (0.26) suggesting that high seasonal groundwater storage that helps to sustain baseflow is a common phenomenon in alpine watersheds (Figure 7). Although in Switzerland the recession periods in the Jura and on the Plateau are shorter than the winter recession in high alpine areas, their mean FI values (0.17 for Jura and 0.19 for Plateau) are lower than for alpine watersheds (0.23; Figure 7). This suggests that alpine watersheds can be more effective in storing and redistributing water seasonally than lowland watersheds. This conclusion is also supported by the study of Staudinger et al. (2017) that found the highest dynamic storage magnitudes for high-altitude catchments.

5. Summary and Conclusion

The study demonstrates that it is possible to quantify dynamic groundwater storage with a narrow range of uncertainty even for high-altitude alpine catchments with difficult access and very complex geological conditions. The key data requirements of the method are a detailed SWE inventory at the onset of snowmelt and stream discharge measurements that capture the entire catchment outflow. An accurate quantification of

other terms of the water balance, especially evapotranspiration and sublimation, is less important as the calculation is carried out over a short period, and their influence on the water balance is fairly small. Compared to previous approaches, the airborne LIDAR-acquisition makes it possible to map SWE in the entire catchment even if topographic constraints and avalanche hazards limit access to site. The comparison of two methods to quantify snow densities indicate that the proposed approach can even be implemented if no access to the study region at all is possible during winter.

The application of the method to Réchy site revealed that, even in high-altitude alpine catchments, substantial "suspended" groundwater storage occurs. At the site, the groundwater storage increase during snowmelt amounted to half of the SWE present in the catchment at the onset of snowmelt. This large fraction clearly highlights the potential of high alpine aquifers to seasonally redistribute water. The stored groundwater persisted over months and was steadily released during a 7-month-long recession period at a rate of 40–60 mm/month. At the end of the recession period, the catchment still yielded 0.9 mm/day. Hence, groundwater storage strongly stabilizes catchment outflow in an environment where stream runoff is otherwise extremely dynamic due to the steep topographic gradients. Given the high groundwater storage capacity, earlier snowmelt due to increasing temperature would be expected to have limited influence on the catchment outflow during summer and fall dry periods.

At the study site, high groundwater storage seems to be related to the subhorizontal subsurface topography of a composite bedrock aquifer, which is in stark contrast to the steep surface topography. In addition, sequential groundwater storage likely plays an important role in delaying runoff from the catchment and the presence of material with an appropritae permeability to retrain water despite steeper gardients. The absence of a tree cover at high alpine site likely contributes to the subsequent groundwater availability for baseflow rather than being "lost" by evapotranspiration. Approximate data from other alpine sites suggest that dynamic groundwater storage in the indicated range might be common in such settings. However, depending on the geological conditions, groundwater storage can also be smaller as shown for the Opabin site. These studies highlight the need for detailed 3-D geological analysis for development of appropriate conceptual models as a basis for water resources management and climate impact studies.

Overall, the project demonstrates that dynamic groundwater storage in high alpine area deserves more attention as it has likely a strong influence on how alpine catchments respond to a later onset of snow accumulation in fall and earlier snowmelt due to climate warming. The study also demonstrate that a complex geology and limited site access are no hurdle to quantify dynamic groundwate storage reliabily.

Acknowledgments
The authors would like to thank Jérôme Tavernier for his contributions to the data acquisition. Robert Costa and Laurent Marguet from UNINE and the members of the Crealp, especially Éric Travaglini, are acknowledge for supporting the field work. Part of this project was funded by the Service of the environment of Canton Valais within the framework of project Interreg STRADA-Programma di cooperazione transfrontaliera Italia Svizzera 2007–2013 and by the the Swiss National Science Foundation as part of the PNR61 programme. The authors acknowledge the comments of Hayashi Masaki and two anonomous reviewers that greatly helped to improve the manuscript and Roland Purtschert from University of Berne for his support of the groundwater dating. The experimental date can be accessed on Zenodo (DOI: 10.5281/zenodo.2552093). The autors declare no conflicts of interests.

References

Allen, R. G., Pereira, L. S., Raes, D., & Smith, M. (1998). *Crop evapotranspiration—Guidelines for computing crop water requirements*, (D05109). Roma: FAO.

Andermann, C., Longuevergne, L., Bonnet, S., Crave, A., Davy, P., & Gloaguen, R. (2012). Impact of transient groundwater storage on the discharge of Himalayan rivers. *Nature Geoscience*, *5*(2), 127–132.

Bales, R. C., Molotch, N. P., Painter, T. H., Dettinger, M. D., Rice, R., & Dozier, J. (2006). Mountain hydrology of the western United States. *Water Resources Research*, *42*, W08432. https://doi.org/10.1029/2005WR004387

Baraer, M., Mark, B. G., McKenzie, J. M., Condom, T., Bury, J., Huh, K.-I., et al. (2012). Glacier recession and water resources in Peru's Cordillera Blanca. *Journal of Glaciology*, *58*(207), 134–150.

Baraer, M., McKenzie, J., Mark, B. G., Gordon, R., Bury, J., Condom, T., et al. (2015). Contribution of groundwater to the outflow from ungauged glacierized catchments: A multi-site study in the tropical Cordillera Blanca, Peru. *Hydrological Processes*, *29*(11), 2561–2581. https://doi.org/10.1002/hyp.10386

Baraer, M., McKenzie, J. M., Mark, B. G., Bury, J., & Knox, S. (2009). Characterizing contributions of glacier melt and groundwater during the dry season in a poorly gauged catchment of the Cordillera Blanca (Peru). *Advances in Geosciences*, *22*, 41–49.

Barnett, T. P., Adam, J. C., & Lettenmaier, D. P. (2005). Potential impacts of a warming climate on water availability in snow-dominated regions. *Nature*, *438*(7066), 303–309.

Beniston, M. (2012). Impacts of climatic change on water and associated economic activities in the Swiss Alps. *Journal of Hydrology*, *412-413*, 291–296.

Beniston, M., Keller, F., Koffi, B., & Goyette, S. (2003). Estimates of snow accumulation and volume in the Swiss Alps under changing climatic conditions. *Theoretical and Applied Climatology*, *76*(3), 125–140.

Beniston, M., & Stoffel, M. (2014). Assessing the impacts of climatic change on mountain water resources. *Science of the Total Environment*, *493*, 1129–1137.

Beyerle, U., Aeschbach-Hertig, W., Imboden, D. M., Baur, H., Graf, T., & Kipfer, R. (2000). A mass spectrometric system for the analysis of noble gases and tritium from water samples. *Environmental Science & Technology*, *34*(10), 2042–2050.

Burn, D. H., Buttle, J. M., Caissie, D., MacCulloch, G., Spence, C., & Stahl, K. (2008). The processes, patterns and impacts of low flows across Canada. *Canadian Water Resources Journal*, *33*(2), 107–124.

Carlier, C., Wirth, S. B., Cochand, F., Hunkeler, D., & Brunner, P. (2018). Geology controls streamflow dynamics. *Journal of Hydrology*, *566*, 756–769.

Challandes, A. (1992). Géologie générale et structurale dans le sud et ouest du val de Réchy (Pennique, Valais-Suisse) [General and structural geology in the southern and western part of the Réchy valley (Pennine, Valais-Switzerland)], Université de Neuchâtel, Neuchâtel, Switzerland.
Christensen, N. S., Wood, A. W., Voisin, N., Lettenmaier, D. P., & Palmer, R. N. (2004). The effects of climate change on the hydrology and water resources of the Colorado River basin. *Climatic Change*, *62*(1), 337–363.
Clow, D. W., Schrott, L., Webb, R., Campbell, D. H., Torizzo, A., & Dornblaser, M. (2003). Ground water occurrence and contributions to streamflow in an Alpine Catchment, Colorado Front Range. *Ground Water*, *41*(7), 937–950.
Cowie, R. M., Knowles, J. F., Dailey, K. R., Williams, M. W., Mills, T. J., & Molotch, N. P. (2017). Sources of streamflow along a headwater catchment elevational gradient. *Journal of Hydrology*, *549*, 163–178.
Deems, J. S., Painter, T. H., & Finnegan, D. C. (2013). Lidar measurement of snow depth: A review. *Journal of Glaciology*, *59*(215), 467–479.
DeWalle, D. R., & Rango, A. (2008). *Principles of snow hydrology*. Cambridge: Cambridge University Press.
Dingman, S. L. (2015). *Physical hydrology*. Long Grove IL: Waveland press.
Eaton, A. K., Rouse, W. R., Lafleur, P. M., Marsh, P., & Blanken, P. D. (2001). Surface energy balance of the western and central Canadian subarctic: Variations in the energy balance among five major terrain types. *Journal of Climate*, *14*(17), 3692–3703.
Escher, A., Marthaler, M. & Sartori, M. (2008). Vissoie (Feuille 1307), Federal Office of Topography Swisstopo, Bern, Switzerland.
Finger, D., Heinrich, G., Gobiet, A., & Bauder, A. (2012). Projections of future water resources and their uncertainty in a glacierized catchment in the Swiss Alps and the subsequent effects on hydropower production during the 21st century. *Water Resources Research*, *48*, W02521. https://doi.org/10.1029/2011WR010733
Federal Office of the Environment (2011). Die Niedrigwasser-Datenbank NQStat, Federal Office of the Environment, Bern.
Galleani, L., Vigna, B., Banzato, C., & Russo, S. L. (2011). Validation of a vulnerability estimator for spring protection areas: The VESPA index. *Journal of Hydrology*, *396*(3–4), 233–245.
Glennie, C. (2007). Rigorous 3D error analysis of kinematic scanning LIDAR systems. *Journal of Applied Geodesy*, *1*, 147–157.
Gordon, R. P., Lautz, L. K., McKenzie, J. M., Mark, B. G., Chavez, D., & Baraer, M. (2015). Sources and pathways of stream generation in tropical proglacial valleys of the Cordillera Blanca, Peru. *Journal of Hydrology*, *522*, 628–644.
Haller, T., Hauser, F., & Weingartner, R. (2004). *Atlas Hydrologique de la Suisse [Hydrological Atlas of Switzerland]*. Bern, Switzerland: Federal Office for the Environment, FOEN.
Harmel, R., Cooper, R., Slade, R., Haney, R., & Arnold, J. (2006). Cumulative uncertainty in measured streamflow and water quality data for small watersheds. *The American Society of Agricultural and Biological Engineers*, *49*(3), 689.
Hartzell, P. J., Gadomski, P. J., Glennie, C. L., Finnegan, D. C., & Deems, J. S. (2015). Rigorous error propagation for terrestrial laser scanning with application to snow volume uncertainty. *Journal of Glaciology*, *61*(230), 1147–1158.
Hood, E., Williams, M., & Cline, D. (1999). Sublimation from a seasonal snowpack at a continental, mid-latitude alpine site. *Hydrological Processes*, *13*(12-13), 1781–1797. https://doi.org/10.1002/(SICI)1099-1085(199909)13:12/13<1781::AID-HYP860>3.0.CO;2-C
Hood, J. L., & Hayashi, M. (2015). Characterization of snowmelt flux and groundwater storage in an alpine headwater basin. *Journal of Hydrology*, *521*, 482–497.
Jefferson, A., Nolin, A., Lewis, S., & Tague, C. (2008). Hydrogeologic controls on streamflow sensitivity to climate variation. *Hydrological Processes*, *22*(22), 4371–4385.
Jonas, T., Marty, C., & Magnusson, J. (2009). Estimating the snow water equivalent from snow depth measurements in the Swiss Alps. *Journal of Hydrology*, *378*(1–2), 161–167.
Katsuyama, M., Ohte, N., & Kabeya, N. (2005). Effects of bedrock permeability on hillslope and riparian groundwater dynamics in a weathered granite catchment. *Water Resources Research*, *41*, W01010. https://doi.org/10.1029/2004WR003275
Klaus, J., & McDonnell, J. J. (2013). Hydrograph separation using stable isotopes: Review and evaluation. *Journal of Hydrology*, *505*, 47–64.
Kobierska, F., Jonas, T., Kirchner, J. W., & Bernasconi, S. M. (2015). Linking baseflow separation and groundwater storage dynamics in an alpine basin (Dammagletscher, Switzerland). *Hydrology and Earth System Sciences*, *19*(8), 3681–3693.
Langmuir, D. (1997) *Aqueous environmental geochemistry*. Upper Saddle River, NJ: Prentice-Hall.
Langston, G., Bentley, L. R., Hayashi, M., McClymont, A., & Pidlisecky, A. (2011). Internal structure and hydrological functions of an alpine proglacial moraine. *Hydrological Processes*, *25*(19), 2967–2982.
Larson, L. W., & Peck, E. L. (1974). Accuracy of precipitation measurements for hydrologic modeling. *Water Resources Research*, *10*(4), 857–863.
Lauber, U., Kotyla, P., Morche, D., & Goldscheider, N. (2014). Hydrogeology of an Alpine rockfall aquifer system and its role in flood attenuation and maintaining baseflow. *Hydrology and Earth System Sciences*, *18*(11), 4437–4452.
Lebedev, A. L. (2015). Kinetics of gypsum dissolution in water. *Geochemical International*, *53*(9), 811–824.
Liu, F. J., Williams, M. W., & Caine, N. (2004). Source waters and flow paths in an alpine catchment, Colorado Front Range, United States. *Water Resources Research*, *40*, W09401. https://doi.org/10.1029/2004WR003076
Lugon, R., & Delaloye, R. (2001). Modelling alpine permafrost distribution, Val de Réchy, Valais Alps (Switzerland). *Norwegian Journal of Geography*, *55*, 224–229.
Marthaler, M., Sartori, M., Escher, A.& Meisser, N. (2008). Vissoie (Feuille 1307)- with explanatory text. Swisstopo, O.f.d.t. (ed), Federal Office of Topography swisstopo, Bern, Switzerland.
McClymont, A. F., Hayashi, M., Bentley, L. R., Muir, D., & Ernst, E. (2010). Groundwater flow and storage within an alpine meadow-talus complex. *Hydrology and Earth System Sciences*, *14*(6), 859–872.
McClymont, A. F., Roy, J. W., Hayashi, M., Bentley, L. R., Maurer, H., & Langston, G. (2011). Investigating groundwater flow paths within proglacial moraine using multiple geophysical methods. *Journal of Hydrology*, *399*(1–2), 57–69.
Moore, R. (2004). Introduction to salt dilution gauging for streamflow measurement: Part 1. *Streamline Watershed Management Bulletin*, *7*(4), 20–23.
Muir, D. L., Hayashi, M., & McClymont, A. F. (2011). Hydrological storage and transmission characteristics of an alpine talus. *Hydrological Processes*, *25*(19), 2954–2966.
Nichols, J., Eichinger, W., Cooper, D., J. H. Prueger, Hipps, L., Neale, C. & Bawazir, A. (2004). Comparison of evaporation estimation methods for a riparian area, p. 50, University of Iowa, Iowa City.
Pauritsch, M., Wagner, T., Winkler, G., & Birk, S. (2017). Investigating groundwater flow components in an Alpine relict rock glacier (Austria) using a numerical model. *Hydrogeology Journal*, *25*(2), 371–383.
Paznekas, A., & Hayashi, M. (2016). Groundwater contribution to winter streamflow in the Canadian Rockies. *Canadian Water Resources Journal*, *41*, 484–499.
Pfister, L., Martinez-Carreras, N., Hissler, C., Klaus, J., Carrer, G. E., Stewart, M. K., & McDonnell, J. J. (2017). Bedrock geology controls on catchment storage, mixing, and release: A comparative analysis of 16 nested catchments. *Hydrological Processes*, *31*(10), 1828–1845.

Priestley, C., & Taylor, R. (1972). On the assessment of surface heat flux and evaporation using large-scale parameters. *Monthly Weather Review*, *100*(2), 81–92.
Riegl (2015). Riegl VQ-580 datasheet.
Rohrer, M., Salzmann, N., Stoffel, M., & Kulkarni, A. V. (2013). Missing (in-situ) snow cover data hampers climate change and runoff studies in the Greater Himalayas. *Science of the Total Environment*, *468-469*, S60–S70.
Roy, J., & Hayashi, M. (2009). Multiple, distinct groundwater flow systems of a single moraine-talus feature in an alpine watershed. *Journal of Hydrology*, *373*(1–2), 139–150.
Saunders, I. R., Bailey, W. G., & Bowers, J. D. (1997). Evaporation regimes and evaporation modelling in an alpine tundra environment. *Journal of Hydrology*, *195*(1–4), 99–113.
Sayama, T., McDonnell, J. J., Dhakal, A., & Sullivan, K. (2011). How much water can a watershed store? *Hydrological Processes*, *25*(25), 3899–3908.
Schaad, W. (1995). The origin of Rauhwackes (Cornieules) by the karstification of gypsum. *Eclogae Geologicae Helvetiae*, *88*(1), 59–90.
Sevruk, B. (1974). Correction for the wetting loss of a Hellmann precipitation gauge. *Hydrological Sciences Bulletin*, *19*(4), 549–559.
Sevruk, B. (1997). Regional dependency of precipitation-altitude relationship in the Swiss Alps. *Climatic Change*, *36*(3/4), 355–369. https://doi.org/10.1023/A:1005302626066
Sorg, A., Bolch, T., Stoffel, M., Solomina, O., & Beniston, M. (2012). Climate change impacts on glaciers and runoff in Tien Shan (Central Asia). *Nature Climate Change*, *2*(10), 725–731.
Sovilla, B., McElwaine, J. N., Schaer, M., & Vallet, J. (2010). Variation of deposition depth with slope angle in snow avalanches: Measurements from Vallée de la Sionne. *Journal of Geophysical Research*, *115*, F02016. https://doi.org/10.1029/2009JF001390
Staudinger, M., Stoelzle, M., Seeger, S., Seibert, J., Weiler, M., & Stahl, K. (2017). Catchment water storage variation with elevation. *Hydrological Processes*, *31*(11), 2000–2015.
Stewart, I. T., Cayan, D. R., & Dettinger, M. D. (2004). Changes in snowmelt runoff timing in western North America under abusiness as usual'climate change scenario. *Climatic Change*, *62*(1–3), 217–232.
Strasser, U., Bernhardt, M., Weber, M., Liston, G., & Mauser, W. (2008). Is snow sublimation important in the alpine water balance? *The Cryosphere*, *2*(1), 53–66.
Sueker, J. K., Ryan, J. N., Kendall, C., & Jarrett, R. D. (2000). Determination of hydrologic pathways during snowmelt for alpine/subalpine basins, Rocky Mountain National Park, Colorado. *Water Resources Research*, *36*(1), 63–75. https://doi.org/10.1029/1999WR900296
Sultenfuss, J., Roether, W., & Rhein, M. (2009). The Bremen mass spectrometric facility for the measurement of helium isotopes, neon, and tritium in water. *Isotopes in Environmental and Health Studies*, *45*(2), 83–95. https://doi.org/10.1080/10256010902871929
Tague, C., & Grant, G. E. (2004). A geological framework for interpreting the low-flow regimes of Cascade streams, Willamette River Basin, Oregon. *Water Resources Research*, *40*, W04303. https://doi.org/10.1029/2003WR002629
Tague, C., & Grant, G. E. (2009). Groundwater dynamics mediate low-flow response to global warming in snow-dominated alpine regions. *Water Resources Research*, *45*, WO7421. https://doi.org/10.1029/2008WR007179
Taylor, S., Feng, X. H., Williams, M., & McNamara, J. (2002). How isotopic fractionation of snowmelt affects hydrograph separation. *Hydrological Processes*, *16*(18), 3683–3690.
Tenthorey, G. (1993). Paysage géomorphologique du haut-Val de Réchy (Valais, Suisse) et hydrologie liée aux glaciers rocheux [geomorphological landscape of the Haut-Val de Réchy (Valais, Switzerland) and hydrology linked to rock glaciers]. Doctoral dissertation, Université de Fribourg, Fribourg, Switzerland.
Uchida, T., Miyata, S., & Asano, Y. (2008). Effects of the lateral and vertical expansion of the water flowpath in bedrock on temporal changes in hillslope discharge. *Geophysical Research Letters*, *35*, L15402. https://doi.org/10.1029/2008GL034566
Viviroli, D., Dürr, H. H., Messerli, B., Meybeck, M., & Weingartner, R. (2007). Mountains of the world, water towers for humanity: Typology, mapping, and global significance. *Water Resources Research*, *43*, W07447. https://doi.org/10.1029/2006WR005653
Wiederkehr, M., & Möri, A. (2013). swissALTI3D—A new tool for geological mapping. *Swiss Bulletin for Applied Geology*, *18*(1), 61–69.
Williams, M. W., Brown, A. D., & Melack, J. M. (1993). Geochemical and hydrologic controls on the composition of surface-water in a high-elevation basin, Sierra-Nevada, California. *Limnology and Oceanography*, *38*(4), 775–797. https://doi.org/10.4319/lo.1993.38.4.0775
Winkler, G., Wagner, T., Pauritsch, M., Birk, S., Kellerer-Pirklbauer, A., Benischke, R., et al. (2016). Identification and assessment of groundwater flow and storage components of the relict Schöneben Rock Glacier, Niedere Tauern Range, Eastern Alps (Austria). *Hydrogeology Journal*, 1–17.
World Meteorological Organization (2008). *Guide to hydrological practices volume I: Hydrology—From measurement to hydrological information* (p. 296). Geneva: World Meteorological Organization.